NUMERICAL INVESTIGATION OF OSCILLATING HYPERSONIC SHOCK WAVE BOUNDARY LAYER INTERACTIONS AT DIFFERENT FREQUENCIES

Conference Paper · August 2022

CITATIONS
0

READS
297

3 authors:

Debdoot Ghosh
Imperial College London
6 PUBLICATIONS **5** CITATIONS
SEE PROFILE

Deerajkumar Parthipan
Purdue University
3 PUBLICATIONS **2** CITATIONS
SEE PROFILE

Bibin John
VIT University
46 PUBLICATIONS **604** CITATIONS
SEE PROFILE

PROCEEDINGS OF 23RD ANNUAL CFD SYMPOSIUM

CFD DIVISION (AESI) & ADA

AUGUST 11-12, 2022, BENGALURU, INDIA

NUMERICAL INVESTIGATION OF OSCILLATING HYPERSONIC SHOCK WAVE BOUNDARY LAYER INTERACTIONS AT DIFFERENT FREQUENCIES

Debdoot Ghosh[1], Deerajkumar Parthipan[1], Bibin John[1]

[1]Vellore Institute of Technology (VIT), Vellore, India

ABSTRACT

This work discusses oscillating shock wave boundary layer interaction on a flat plate at 5.8 Mach. The shock generator is a wedge which is free to oscillate with a maximum flow deflection angle of 10 degrees. The frequencies chosen for the study includes 47 Hz, 80 Hz and 100 Hz. The incipient angle for the flow was calculated to be 4.7 degrees, which indicates that the flow separation of the boundary layer due to the shock impingement takes place beyond 4.7 degrees. There was no significant change in the pressure values with changing the frequencies of the shock generator. The flow seems to be separated, indicated by a plateau region in the pressure graph for above angles of 5 degrees, that is, whence the total deflection angle is greater than incipient angle.

Keywords: Shock Oscillation, SBLI, Shock bubble

NOMENCLATURE

P_∞	=	Free stream pressure
T_∞	=	Free stream temperature
M_∞	=	Free stream Mach number
P_g	=	Gauge pressure
ReL	=	Reynolds number for characteristic length L.
Tw	=	Temperature at the wall.
A	=	amplitude of oscillation
C_p	=	pressure coefficient

1. INTRODUCTION

Shock conditions and Shock Wave Boundary Layer Interactions (SWBLI), as depicted in Fig. 1 are common in a hypersonic regime and can pose significant challenges to the operation of air-breathing accelerated hypersonic vehicles like scramjets. The transient effects such as changes in operating conditions can vary the shock strengths and impingement locations, which can lead to the unstarting of the scramjet engine. The SBLI phenomenon can also cause localized heating and pressure levels higher than those predicted by fully turbulent predictions [1]. Furthermore, oscillations of shocks [2] take place in the cowl, isolator, and fuselage owing to the aeroelastic nature of the vehicle. These non-stationary nature of shock conditions can trigger boundary layer transitions [3] resulting in separation and reattachment points, which are often identified as shock bubbles. As shock bubbles result in peak heating, analyzing and locating these shock bubble locations is essential to designing passive and active thermal protection systems. There exists a considerable body of literature on hypersonic SWBLI [4–14], shock unsteadiness [12–20], and shock bubble formation [24–30]. In more holistic studies related to unsteady SWBLI and shock bubble, for instance, Trilling [2] observed changes in bubble shape causing a variation in the separation angle and, consequently, variation in pressure in the reattachment region due increase in mass flow rate in the reattachment point; Pasquariello et al [31] studied shock bubble dynamics coupled with shock motion; in numerical investigations by Poggie, et a [32], separation region unsteadiness was found to coupled strongly with Gortler-like vortices.

This paper is focused on modeling and analyzing the changes in frequencies and their effects on the SWBLI. This is important because SWBLI can cause flow separation on the plate, which can directly affect the maneuverability of the vehicle, given that the shock impinges on a control surface. The incipient angle [33] is the angle of shock impingement after which the boundary layer separation starts. The incipient angle was calculated to be 4.7 degrees for the given flow conditions. FLUENT 2022R2 was chosen for all the numerical analyses for its dynamic meshing capability and accuracy of simulation results when compared to experimental data. Both steady-state and transient numerical studies are carried out to study the SWBLI flow field and the thus formed shock bubble dynamics. A user-defined function was used to define the motion of the shock generator using C language. The user-defined frequencies of 47 Hz, 80 Hz, and 100 Hz were used as the shock generator for this study.

2. GEOMETRY AND MESH

All materials and methods that have been used in the work must be stated clearly. Subtitles should be used when necessary. The 2D geometry was designed in SolidWorks. The design consists of a wedge shock generator and a flat plate as shown in the fig. (1). The shock generator has a semi angle θ_{wf} = 5° and a length of 110 mm. The pivoting point was located at a distance of 36 mm from the tip of the wedge. The meshing was done using ANSYS meshing software.

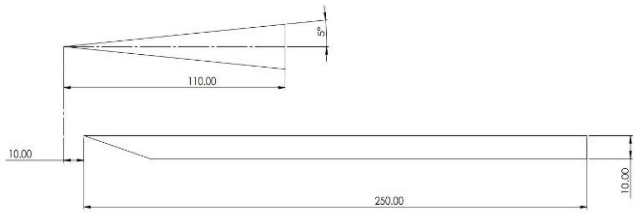

FIGURE 1: SCHEMATIC OF SHOCK WAVE GENERATOR AND FLAT PLATE

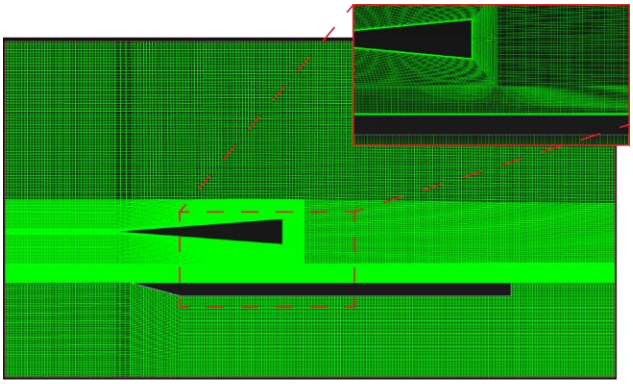

(a) Computational mesh at zero deflection angle

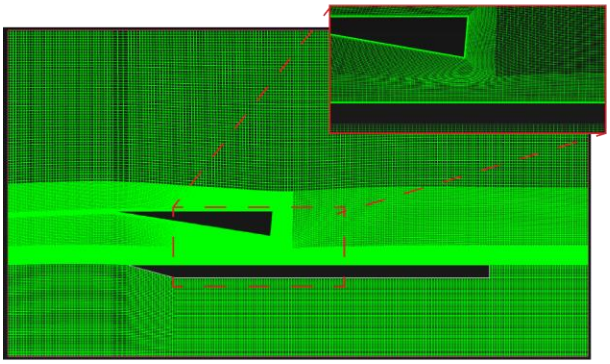

(b) Computational mesh at a non-zero deflection angle

FIGURE 2: SNAPSHOT OF INITIAL MESH AT θ_{wf} = 5°

The initial cell count was 1.52 × 10^5, which indicated a coarse mesh. An initial static CFD simulation was run using ANSYS FLUENT and the pressure values were computed. Mesh refinement was done using mesh adaptation technique with a mesh refinement index of 60 which gave a finer mesh with 7.58 × 10^5 elements.

Dynamic Mesh Operation

To perform the oscillation of the shock generator, a C code based User Defined Function (UDF) has been generated and compiled in ANSYS Fluent which has an inbuilt applet of Visual Studio 7. The angular frequency (ω) is defined in the code as = maximum angle of attack x angular frequency x cos(angular frequency xtime)

$$\omega' = A\omega\cos(\omega t) \tag{1}$$

3. NUMERICAL SETUP

Two-dimensional numerical investigations are carried out to analyse the various flow features. Density based solver along with Advection Upstream Splitting Method (AUSM) is used to approximate the flux functions. Second-order upwind method is used for spatial discretization and first order implicit scheme for temporal discretization. Ansys Fluent is used to solve the transient and compressible 2D flow equations. Navier stokes equation, Energy equation and continuity equation were solved using finite volume method. RANS equations were incorporated with a k-ϵ Realizable turbulence model with standard wall functions. Its improved performance for flows involving rotation, boundary layers under significant adverse pressure gradients, separation, and recirculation led to the selection of the Realizable k-ϵ model. A second order discretization scheme was used. The convergence criteria were set to achieve 10-3 for the scaled residuals.

The transport equations of k-ϵ Realizable turbulence model are given by:

$$\frac{\partial}{\partial t}(\rho k) + \frac{\partial}{\partial x_j}(\rho k u_j) = \frac{\partial}{\partial x_j}\left[\left(\mu + \frac{\mu_t}{\sigma_k}\right)\frac{\partial k}{\partial x_j}\right] + G_k + G_b - \rho\epsilon - Y_M + S_k \tag{2}$$

$$\frac{\partial}{\partial t}(\rho\epsilon) + \frac{\partial}{\partial x_j}(\rho\epsilon u_j) = \frac{\partial}{\partial x_j}\left[\left(\mu + \frac{\mu_t}{\sigma_\epsilon}\right)\frac{\partial \epsilon}{\partial x_j}\right] + \rho C_1 S\epsilon - \rho C_2 \frac{\epsilon^2}{k + \sqrt{\nu\epsilon}} + C_{1\epsilon}\frac{\epsilon}{k}C_{3\epsilon}G_b + S_\epsilon \tag{3}$$

where,

$$C_1 = \max\left[0.43, \frac{\eta}{\eta + 5}\right], \quad \eta = S\frac{k}{\epsilon}, \; S = \sqrt{2S_{ij}S_{ij}}$$

In these equations, G_k represents the generation of turbulence kinetic energy due to mean velocity gradients. $G\omega$ represents the generation of ω. Γ_k and Γ_ω represent the effective diffusivity of k and ω, respectively. Yk and $Y\omega$ represent the dissipation of k

and ω due to turbulence. All of the above terms are calculated as described below. S_k and S_ω are user-defined source terms .

Table 1 BOUNDARY CONDITIONS

Surface	Boundary Type	Boundary Condition
Inlet	Pressure Far-field	P_∞=755Pa, $T_\infty = 75K$, $M_\infty = 5.80$
Outlet	Pressure Outlet	P_0=0Pa

3.1 Numerical Scheme Validation Study

In order to quantify the reliability of numerical scheme and as well as CFD solver used, ANSYS Fluent, a comparative study was carried between current investigation and experimental study by Currao et.al (2021). The results seem to match almost accurately with the experimental studies.

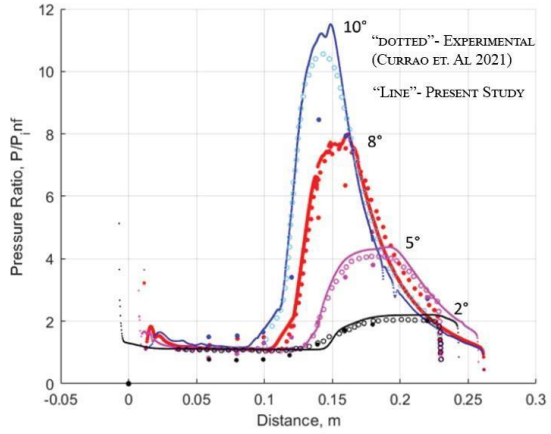

FIGURE 3: COMPARISON OF EXPERIMENTAL DATA WITH PRESENT CFD STUDY. CURRAO ET AL. [2]

3.2 Mesh Independent Study

The accuracy of numerical results obtained are highly dependent on the quality of mesh used. Finer the grid, the better would be the accuracy. However, due to computational limits an optimal mesh has to be generated which can give high-fidelity results exploiting available computational resources. In order to determine a suitable mesh for the present study, aforementioned numerical configuration is used with free-stream flow conditions as in the Table (1) for three different meshes of the same geometry but consisting of different cell counts - Coarse mesh with 0.78 million cells, Medium Mesh with 1.24 million cells, and Fine mesh with 0.65 million cells. After the iterative solutions converged with a residue of order of 10^{-5}.

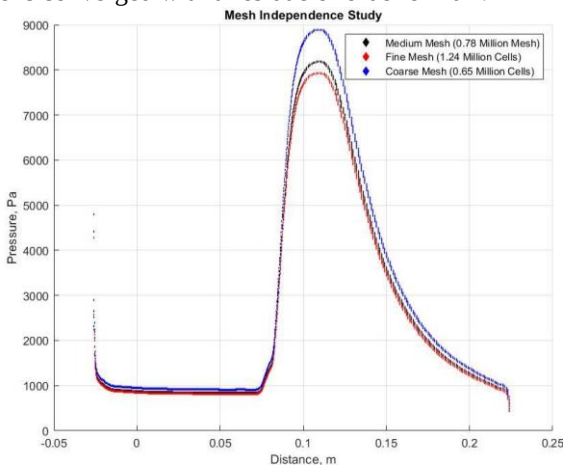

FIGURE 4: COMPARISON OF PRESSURE DISTRIBUTION ALONG THE FLAT PLATE

For each of three cases, pressure distribution along the flat plate is plotted and compared for each of three different cases. As the figure depicts, pressure distribution is almost the same for every case with a little to no deviation near the region of the region of formation of separation bubble. Therefore, the medium mesh is used for further investigations, considering the accuracy of results obtained from it and the computational resources it needs.

4. RESULTS

4.1 Steady State Flow Analysis

The images present the typical features of a SWBLI, namely, impinging shock (area 1), separation shock (area 2), the expansion fan just above the separated region (area 3), and reattachment shock (area 4). Additionally, there are also the leading-edge shock (area 5) and the expansion fan (area 6) generated at the trailing edge of the shock generator. The flow separates for every flow-deflection angle other than α_s =2 deg, where waves 2, 3, and 4 almost coalesce.

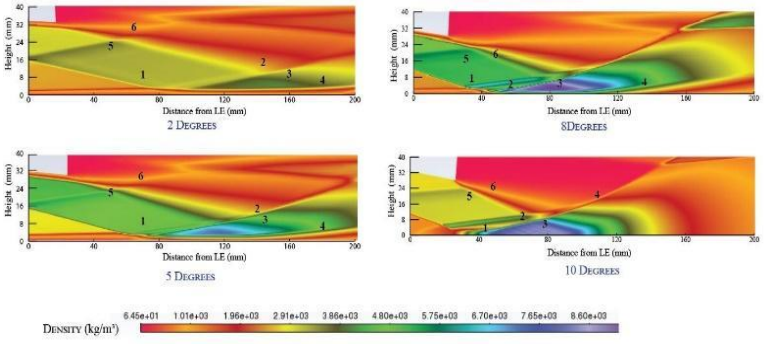

FIGURE 5: DENSITY CONTOUR PLOTS OF THE FLOW FIELD AT A DIFFERENT ANGLES OF ATTACKS

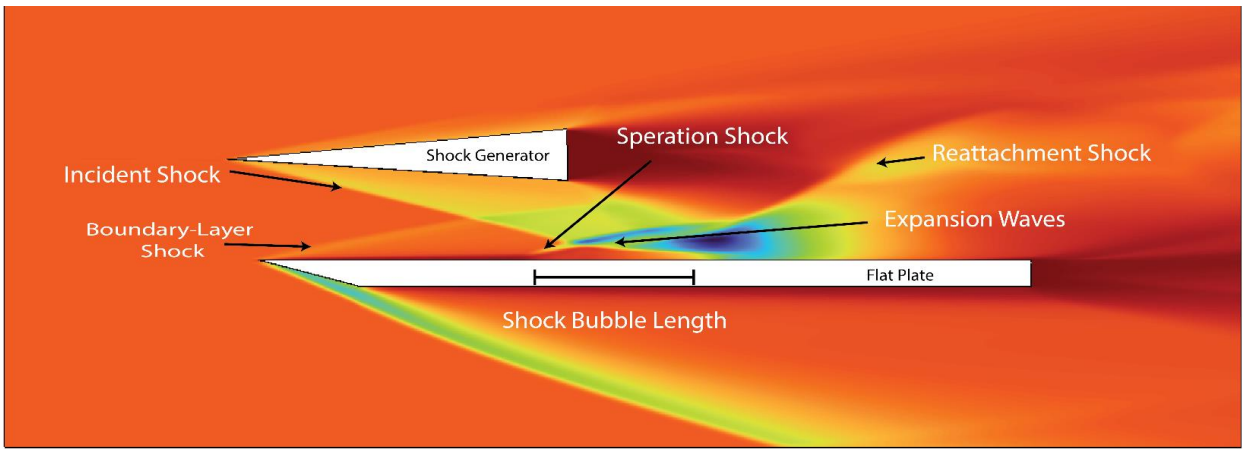

FIGURE 6: HYPERSONIC SWBLI FLOW-FIELD DESCRIPTION

4.2 Incipient angle calculation

The angle of impingement after which the boundary layer separation takes place is known as the incipient angle. The formulas for the incipient angle calculations are given below. The incipient angle for the flow conditions was found to be 4.7 degrees.

$$\theta_{is} = \frac{80\sqrt{\chi_L}}{M_\infty} \qquad (4)$$

where, χ_L is the viscous interaction parameter at the flat plate-ramp junction, and is given by $\overline{\chi_L} = M_\infty^3\sqrt{C}/\sqrt{Re_L}$ where,

$$C = \frac{\mu_W T_\infty}{\mu_\infty T_W}$$

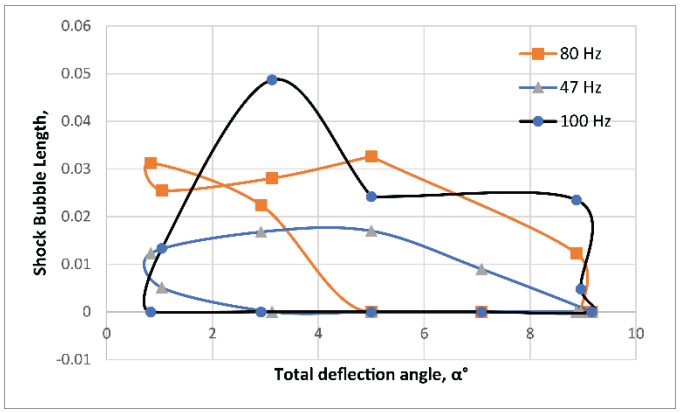

FIGURE 7: VARIATION OF SHOCK BUBBLE LENGTH WITH TOTAL DEFLECTION ANGLE

4.3 Transient Flow Analysis

Density contours depicting various flow features as discussed in section 4.1 are observed in the transient cases and presented in Fig. 9 at zero, maximum, and minimum deflection angles.

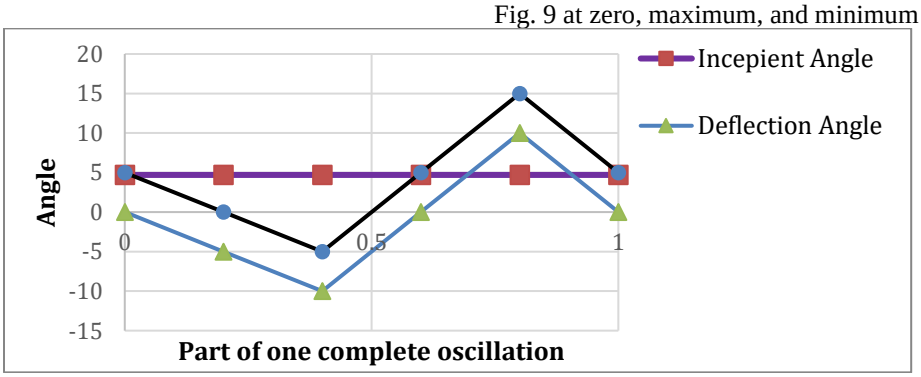

FIGURE 8: VARIATION OF INCIPIENT ANGLE, DEFLECTION ANGLE, AND TOTAL DEFLECTION ANGLE WITH ELAPSED PART OF ONE OSCILLATION OF THE SHOCK GENERATOR

And, variation of incipient angle, deflection angle, and total deflection angle with elapsed part of one oscillation of the shock generator is presented in Fig. 8

I. At 47 Hz

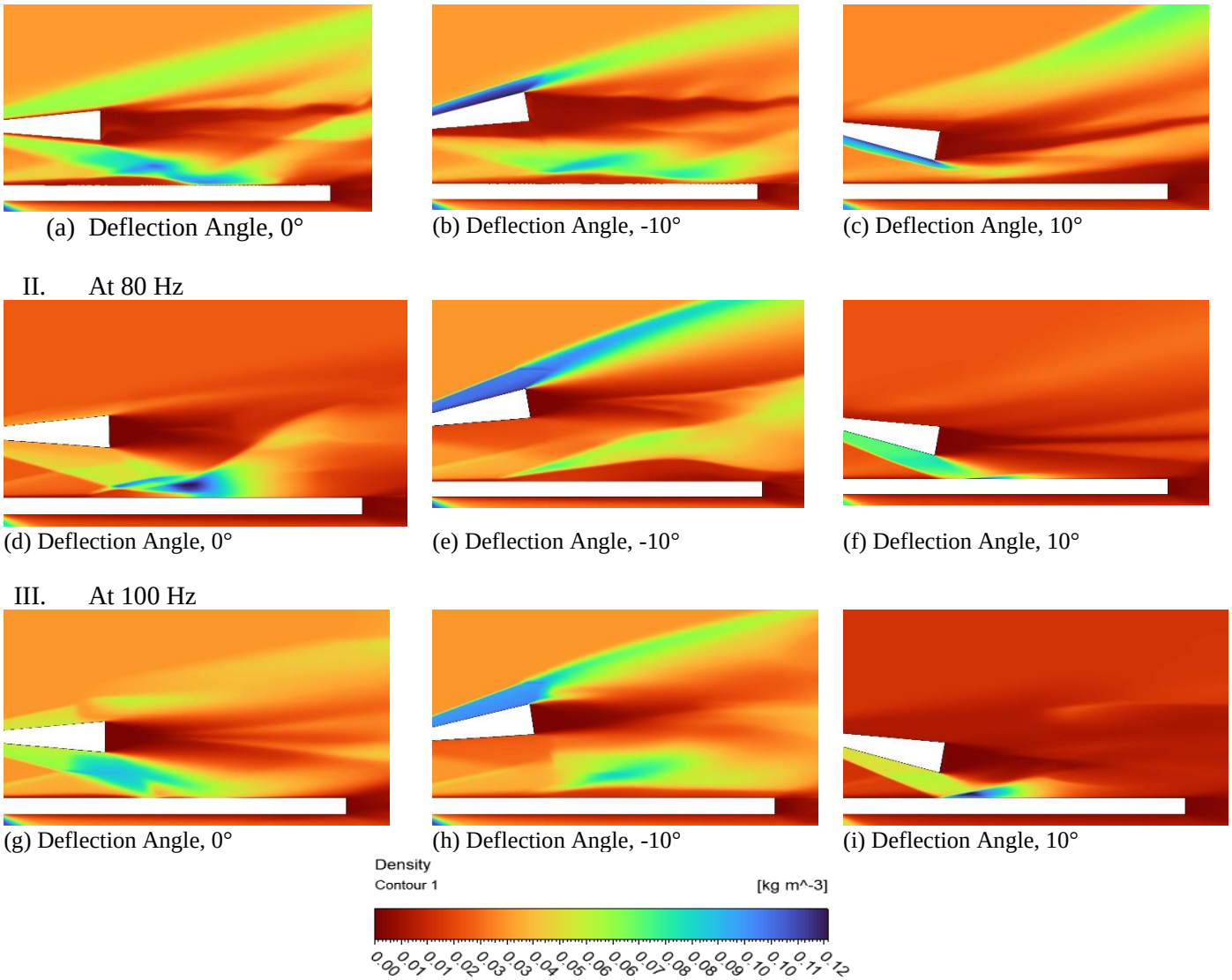

(a) Deflection Angle, 0° (b) Deflection Angle, -10° (c) Deflection Angle, 10°

II. At 80 Hz

(d) Deflection Angle, 0° (e) Deflection Angle, -10° (f) Deflection Angle, 10°

III. At 100 Hz

(g) Deflection Angle, 0° (h) Deflection Angle, -10° (i) Deflection Angle, 10°

FIGURE 9: DENSITY CONTOURS AT DIFFERENT FREQUIENCIES AND ANGLE OF DEFLECTION

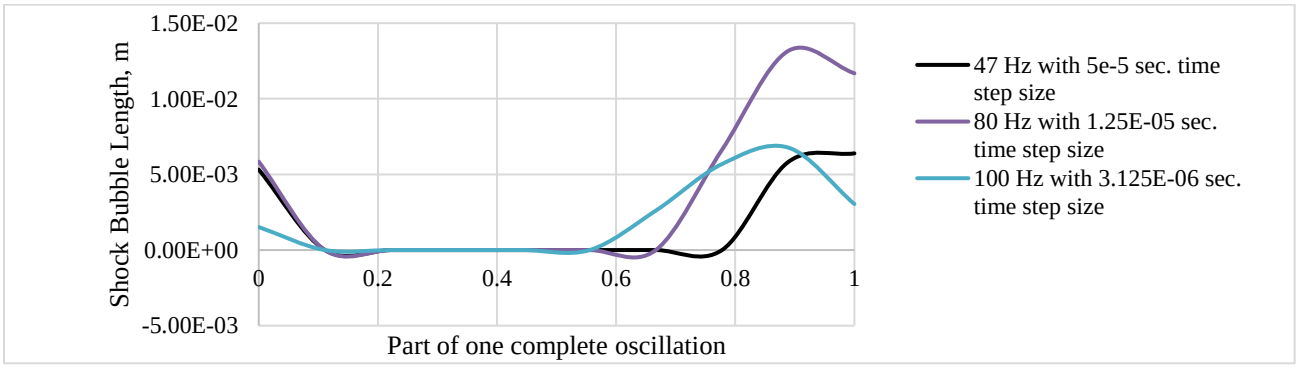

FIGURE 10: SHOCK BUBBLE LENGTH VARIATION FOR DIFFERENT FREQUENCY OF SHOCK GENERATOR OSCILLATION

Shock bubble formation as predicted by incipient angle calculation, that is, when the total deflection is greater than the incipient angle there will flow separation and shock bubble formation is evident from the results obtained for different frequencies of oscillation of shock generator as presented in Fig. 10. For example, a detailed study of the flow field for 80 Hz frequency case is represented in Fig.11, where it can observed shock bubble extensive is evident whenever there is negative wall shear stress on the flat plate obtained.

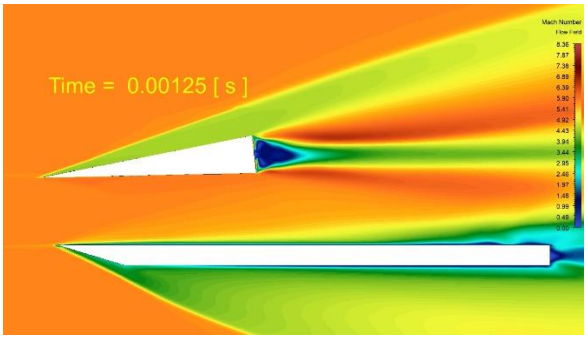

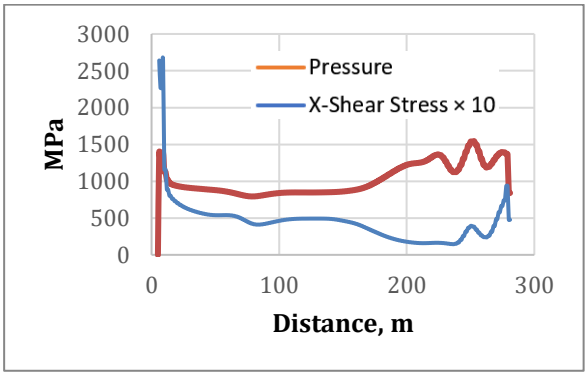

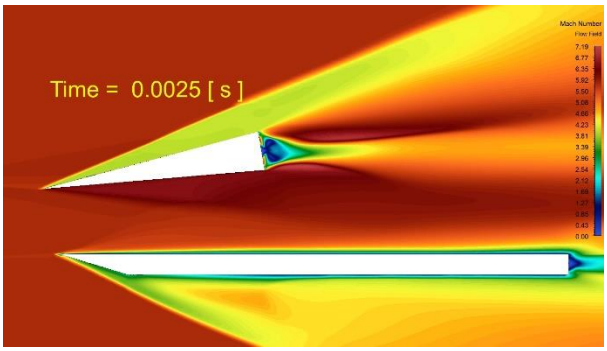

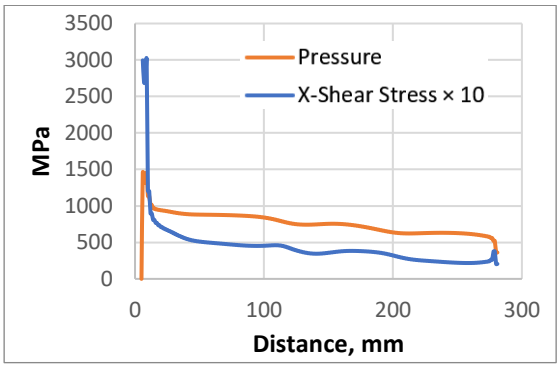

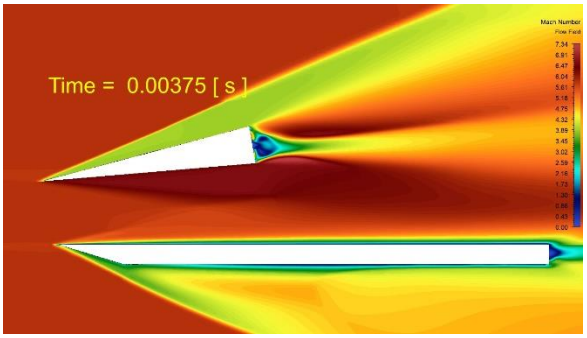

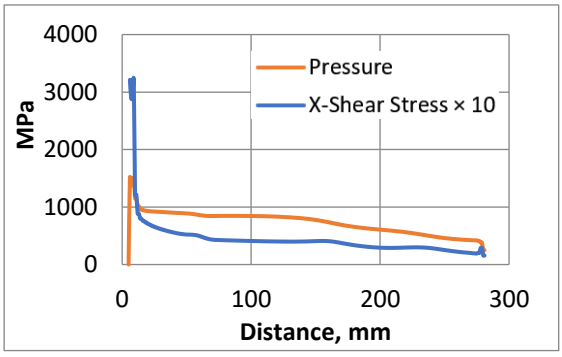

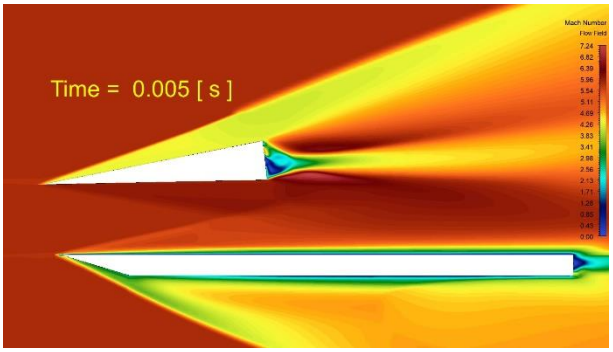

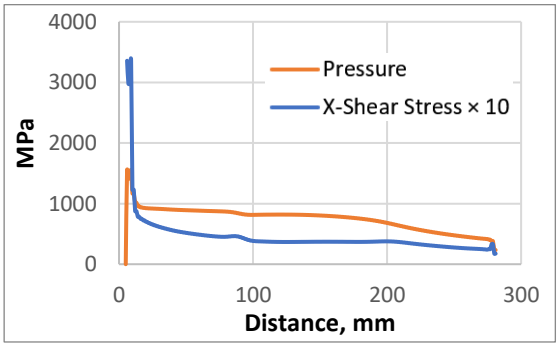

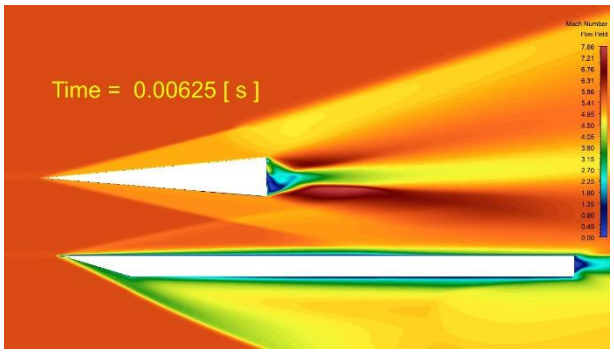
Time = 0.00625 [s]

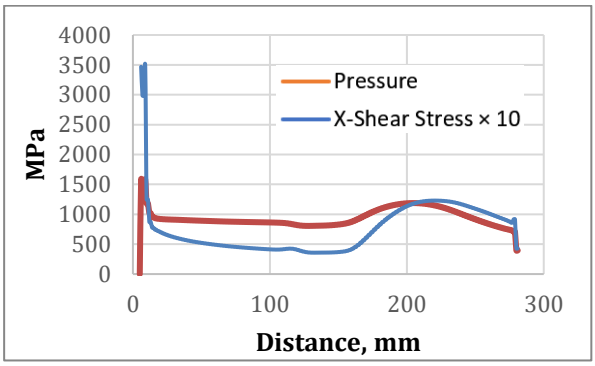
4000
3500
3000
2500
2000
1500
1000
500
0
MPa
Pressure
X-Shear Stress × 10
0
100
200
300
Distance, mm

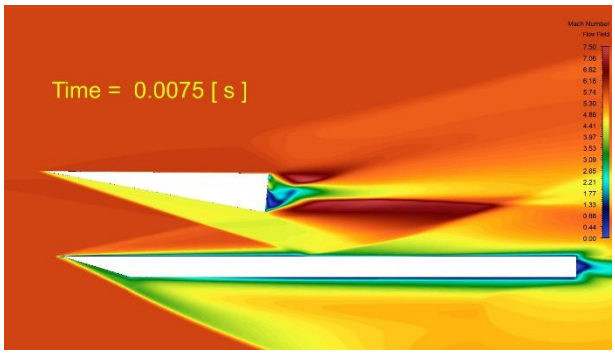
Time = 0.0075 [s]

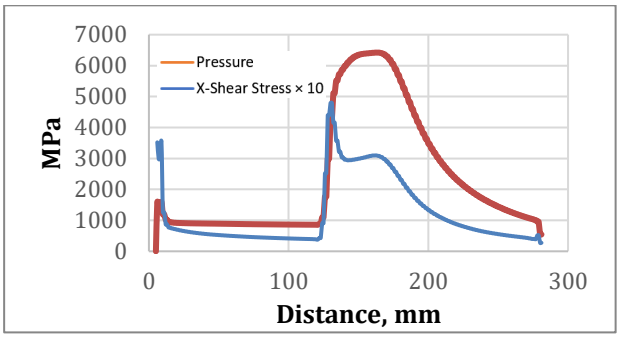
7000
6000
5000
4000
3000
2000
1000
0
MPa
Pressure
X-Shear Stress × 10
0
100
200
300
Distance, mm

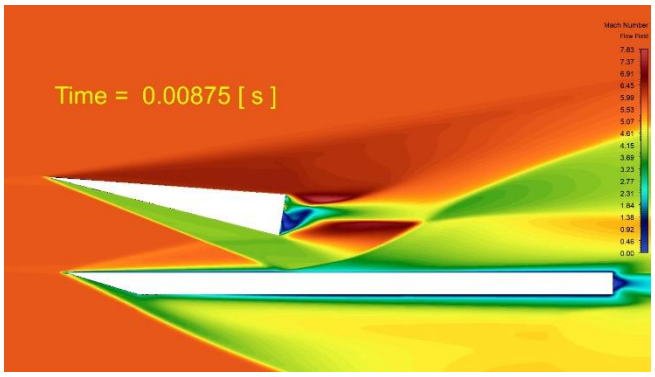
Time = 0.00875 [s]

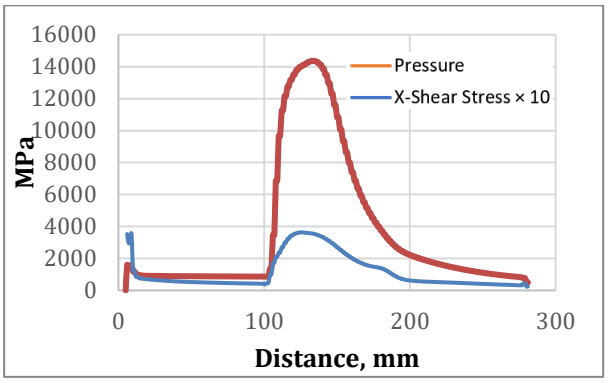
16000
14000
12000
10000
8000
6000
4000
2000
0
MPa
Pressure
X-Shear Stress × 10
0
100
200
300
Distance, mm

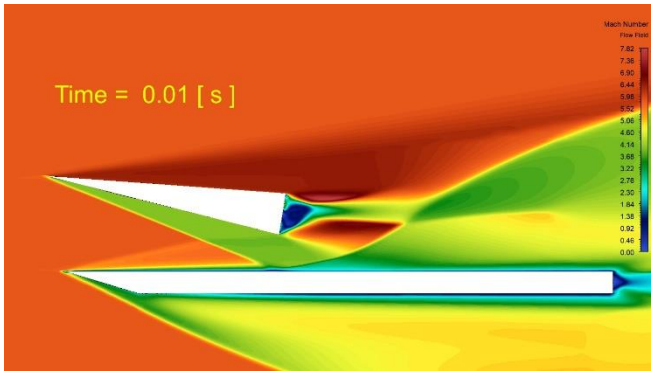
Time = 0.01 [s]

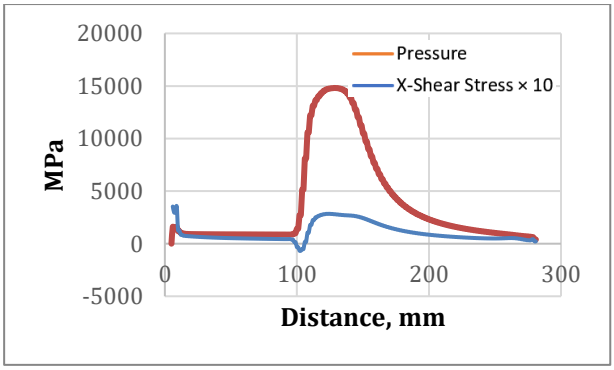
20000
15000
10000
5000
0
-5000
MPa
Pressure
X-Shear Stress × 10
0
100
200
300
Distance, mm

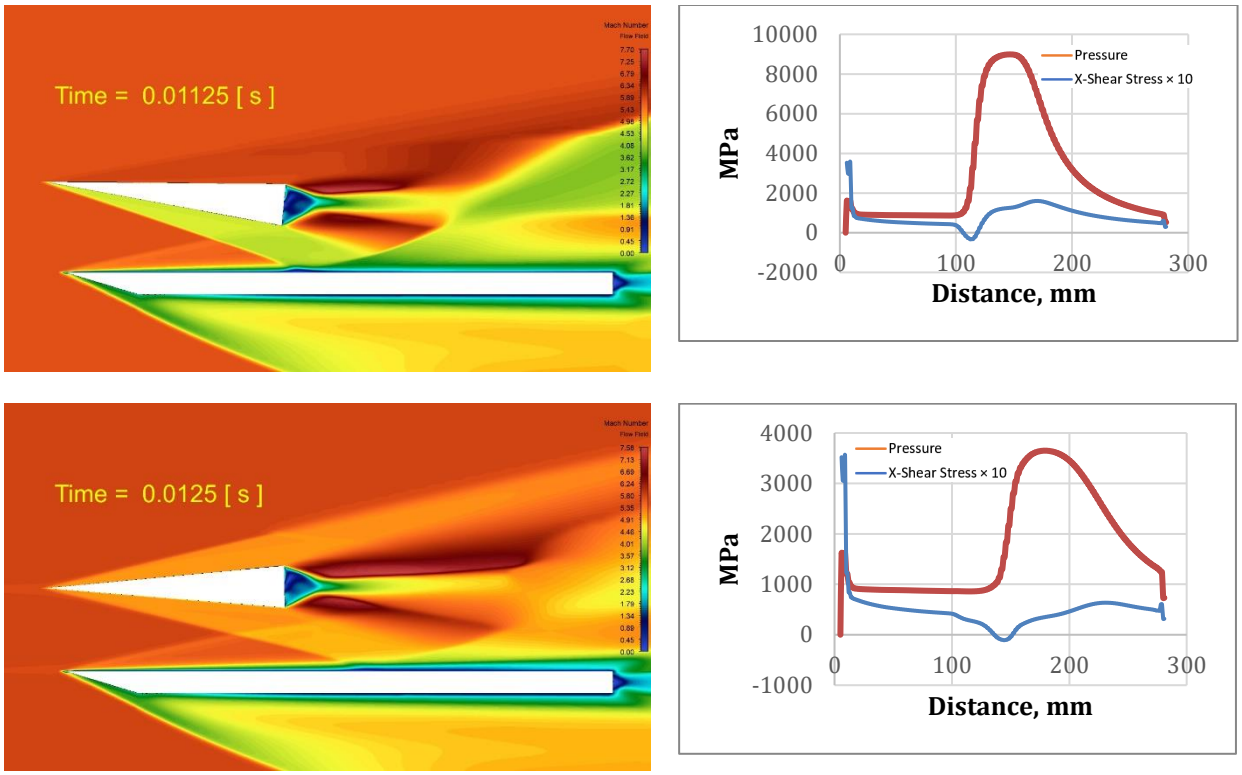

FIGURE 11: FLOW FIELDS, PRESSURE, AND X-SHEAR STRESS VARIATIONS ON THE FLAT PLATE AT DIFFERENT TIMES DURING THE TRANSIENT ANALYSIS AT 80 HZ.

5. CONCLUSION

The study presents an oscillating SWBLI on a flat plate at 5.8 Mach with different frequencies of 47 Hz, 80 Hz, and 100 Hz. In steady-state cases, the angles of impingement were considered to be 2 degrees, 5 degrees, 8 degrees, and 10 degrees. In these SWBLI problems, an oblique shock impinged on a flat plate, promoting separation and boundary-layer transition. The static results matched with the experimental study by Currao et.al (2021) [34]. Mesh independent study shows that the results vary slightly with the size of the mesh. The better-quality mesh gave more accurate results. Transient simulations were carried out to study the dynamic characteristics of the SWBLI. Different frequencies were modeled to the shock generator, using a User-defined function (UDF) in ANSYS FLUENT and dynamic meshing. The pressure plateau that indicates separation is observed at every angle after 5 degrees.

REFERENCES

[1] "Aerothermodynamics – A Critical Review at DLR - ScienceDirect" [Online]. Available: https://www.sciencedirect.com/science/article/abs/pii/S1270963803000361?via%3Dihub. [Accessed: 08-Aug-2022].

[2] Trilling, L., 1958, "Oscillating Shock Boundary-Layer Interaction," Journal of the Aerospace Sciences, **25**(5), pp. 301–304.

[3] "On the Görtler Instability of Boundary Layers - ScienceDirect" [Online]. Available: https://www.sciencedirect.com/science/article/abs/pii/037604219190006P?via%3Dihub. [Accessed: 08-Aug-2022].

[4] Leidy, A. N., Neel, I. T., Tichenor, N. R., and Bowersox, R. D., 2020, "High-Speed Schlieren Imaging of Cylinder-Induced Hypersonic-Shock-Wave–Boundary-Layer Interactions," AIAA Journal, **58**(7), pp. 3090–3099.

[5] Kota, S., and Subbaraju, P., 2019, "Computational Analysis of Shockwave–Boundary Layer Interaction at Hypersonic Speeds," International Journal of Computer Aided Manufacturing, **5**(2), pp. 1–25.

[6] Chang, E. W. K., Chan, W. Y., McIntyre, T. J., and Veeraragavan, A., 2021, "Hypersonic Shock Impingement on a Heated Flat Plate at Mach 7 Flight Enthalpy," Journal of Fluid Mechanics, **908**.

[7] John, B., 2014, "Numerical Investigations of Shock Wave Boundary Layer Interaction in Hypersonic Flows," Ph.D. Thesis.

[8] John, B., Kulkarni, V. N., and Natarajan, G., 2014, "Shock Wave Boundary Layer Interactions in Hypersonic Flows,"

International Journal of Heat and Mass Transfer, **70**, pp. 81–90.

[9] John, B., Surendranath, S., Natarajan, G., and Kulkarni, V., 2016, "Analysis of Dimensionality Effect on Shock Wave Boundary Layer Interaction in Laminar Hypersonic Flows," International Journal of Heat and Fluid Flow, **62**, pp. 375–385.

[10] Zuppardi, G., and Boffa, C., 2012, "Effects of Rarefaction on the Shock Wave/Boundary Layer Interaction in Hypersonic Regime," *AIP Conference Proceedings*, American Institute of Physics, pp. 673–679.

[11] Ritos, K., Kokkinakis, I. W., and Drikakis, D., 2018, "Physical Insight into a Mach 7.2 Compression Corner Flow," *2018 AIAA Aerospace Sciences Meeting*, p. 1810.

[12] White, M. E., and Ault, D. A., 1996, "Expansion Corner Effects on Hypersonic Shock Wave/Turbulent Boundary-Layer Interactions," Journal of propulsion and power, **12**(6), pp. 1169–1173.

[13] Bhattrai, S., McQuellin, L., Currao, G. M., Neely, A., and Buttsworth, D., 2018, "Influence of Hypersonic Fluid-Structure Interaction on the Control Authority of a Trailing-Edge Flap," *22nd AIAA International Space Planes and Hypersonics Systems and Technologies Conference*, p. 5265.

[14] Settles, G. S., and Dodson, L. J., 1994, "Supersonic and Hypersonic Shock/Boundary-Layer Interaction Database," AIAA journal, **32**(7), pp. 1377–1383.

[15] Verma, S., and Koppenwaller, G., 2001, "Study of Flow Unsteadiness in a Hypersonic SWBLI Flowfield on a HAC Model," *39th Aerospace Sciences Meeting and Exhibit*, p. 566.

[16] Sawant, S. S., Tumuklu, O., Theofilis, V., and Levin, D. A., 2022, "Linear Instability of Shock-Dominated Laminar Hypersonic Separated Flows," *IUTAM Laminar-Turbulent Transition*, Springer, pp. 651–660.

[17] Verma, S., and Koppenwallner, G., 2002, "Unsteady Separation in Flare-Induced Hypersonic Shock-Wave Boundary-Layer Interaction Flowfield," Journal of spacecraft and rockets, **39**(3), pp. 467–470.

[18] Pasha, A. A., and Sinha, K., 2012, "Simulation of Hypersonic Shock/Turbulent Boundary-Layer Interactions Using Shock-Unsteadiness Model," Journal of Propulsion and Power, **28**(1), pp. 46–60.

[19] Yamamoto, S., Kano, S., and Daiguji, H., 1998, "An Efficient CFD Approach for Simulating Unsteady Hypersonic Shock–Shock Interference Flows," Computers & fluids, **27**(5–6), pp. 571–580.

[20] Zhong, X., 1994, "Application of Essentially Nonoscillatory Schemes to Unsteady Hypersonic Shock-Shock Interference Heating Problems," AIAA journal, **32**(8), pp. 1606–1616.

[21] Tumuklu, O., Theofilis, V., and Levin, D. A., 2018, "On the Unsteadiness of Shock–Laminar Boundary Layer Interactions of Hypersonic Flows over a Double Cone," Physics of Fluids, **30**(10), p. 106111.

[22] McNamara, J. J., Crowell, A. R., Friedmann, P. P., Glaz, B., and Gogulapati, A., 2010, "Approximate Modeling of Unsteady Aerodynamics for Hypersonic Aeroelasticity," Journal of Aircraft, **47**(6), pp. 1932–1945.

[23] Lind, C. A., and Lewis, M. J., 1995, "Unsteady Characteristics of a Hypersonic Type IV Shock Interaction," Journal of aircraft, **32**(6), pp. 1286–1293.

[24] Kane, A., and Peetala, R., 2020, "Numerical Investigation of the Transient Nature of a Laminar Separation Bubble in Hypersonic Flow," Fluid Dynamics, **55**(4), pp. 511–524.

[25] Jegadheeswaran, S., Kannan, R., and others, "Control of Subsonic Separation Bubble in Hypersonic Intake Using Perforated Wall."

[26] Sriram, R., and Jagadeesh, G., 2015, "Correlation for Length of Impinging Shock-Induced Large Separation Bubble at Hypersonic Speed," AIAA Journal, **53**(9), pp. 2771–2776.

[27] Sriram, R., Srinath, L., Devaraj, M. K. K., and Jagadeesh, G., 2016, "On the Length Scales of Hypersonic Shock-Induced Large Separation Bubbles near Leading Edges," Journal of Fluid Mechanics, **806**, pp. 304–355.

[28] Jiao, X., Chang, J., Wang, Z., and Yu, D., 2017, "Numerical Study on Hypersonic Nozzle-Inlet Starting Characteristics in a Shock Tunnel," Acta Astronautica, **130**, pp. 167–179.

[29] Balakumar, P., Zhao, H., and Atkins, H., 2005, "Stability of Hypersonic Boundary Layers over a Compression Corner," AIAA journal, **43**(4), pp. 760–767.

[30] Bleilebens, M., and Olivier, H., 2006, "On the Influence of Elevated Surface Temperatures on Hypersonic Shock Wave/Boundary Layer Interaction at a Heated Ramp Model," Shock Waves, **15**(5), pp. 301–312.

[31] "Unsteady Effects of Strong Shock-Wave/Boundary-Layer Interaction at High Reynolds Number | Journal of Fluid Mechanics | Cambridge Core" [Online]. Available: https://www.cambridge.org/core/journals/journal-of-fluid-mechanics/article/abs/unsteady-effects-of-strong-shockwaveboundarylayer-interaction-at-high-reynolds-number/4E41E6616ADC85D0CF30DB02A39BBFE9. [Accessed: 08-Aug-2022].

[32] Poggie, J., Bisek, N. J., Kimmel, R. L., and Stanfield, S. A., 2015, "Spectral Characteristics of Separation Shock Unsteadiness," AIAA Journal, **53**(1), pp. 200–214.

[33] Dou, H.-S., Khoo, B. C., and Yeo, K. S., 2006, "Incipient Separation in Shock Wave/Boundary Layer Interactions as Induced by Sharp Fin," Shock Waves, **15**(6), pp. 425–436.

[34] "Hypersonic Oscillating Shock-Wave/Boundary-Layer Interaction on a Flat Plate | AIAA Journal" [Online]. Available: https://arc.aiaa.org/doi/10.2514/1.J059590. [Accessed: 08-Aug-2022].